

---

*This copy is for your personal, non-commercial use only.*

---

If you wish to distribute this article to others, you can order high-quality copies for your colleagues, clients, or customers by [clicking here](#).

Permission to republish or repurpose articles or portions of articles can be obtained by following the guidelines [here](#).

**The following resources related to this article are available online at [www.sciencemag.org](http://www.sciencemag.org) (this information is current as of September 27, 2014 ):**

**Updated information and services**, including high-resolution figures, can be found in the online version of this article at:

<http://www.sciencemag.org/content/345/6204/1587.full.html>

**Supporting Online Material** can be found at:

<http://www.sciencemag.org/content/suppl/2014/08/21/science.1260279.DC1.html>

A list of selected additional articles on the Science Web sites **related to this article** can be found at:

<http://www.sciencemag.org/content/345/6204/1587.full.html#related>

This article **cites 30 articles**, 2 of which can be accessed free:

<http://www.sciencemag.org/content/345/6204/1587.full.html#ref-list-1>

This article appears in the following **subject collections**:

Geochemistry, Geophysics

[http://www.sciencemag.org/cgi/collection/geochem\\_phys](http://www.sciencemag.org/cgi/collection/geochem_phys)

Impact of Star Formation," project area B3. H.S.P.M. is very grateful to the Bundesministerium für Bildung und Forschung for support through projects FKZ 500F0901 (ICC HIFI *Herschel*) and 05A11PK3 (ALMA ARC Node). R.T.G. acknowledges support from the NASA Astrophysics Theory Program through grant NNX11AC38G. This paper makes use of the following ALMA data: ADS/JAO.ALMA#2011.0.00017.S. ALMA is a partnership of the European Southern Observatory (ESO) (representing its member states), NSF (USA), and National Institutes of Natural Sciences

(Japan), together with National Research Council (Canada) and National Science Council and Academia Sinica Institute of Astronomy and Astrophysics (Taiwan), in cooperation with the Republic of Chile. The Joint ALMA Observatory is operated by ESO, Associated Universities Incorporated/National Radio Astronomy Observatory, and National Astronomical Observatory of Japan. The interferometric data are available in the ALMA archive at <https://almascience.eso.org/aq/>. The chemical model input files are located at [www.astro.cornell.edu/~rgarrod/resources](http://www.astro.cornell.edu/~rgarrod/resources).

# SUPPLEMENTARY MATERIALS

[www.sciencemag.org/content/345/6204/1584/suppl/DC1](http://www.sciencemag.org/content/345/6204/1584/suppl/DC1)  
Materials and Methods  
Figs. S1 to S6  
Tables S1 and S2  
References (17–30)

29 May 2014; accepted 20 August 2014  
10.1126/science.1256678

## REMOTE HYDROLOGY

# Ongoing drought-induced uplift in the western United States

Adrian Antal Borsa,<sup>1\*</sup> Duncan Carr Agnew,<sup>1</sup> Daniel R. Cayan<sup>1,2</sup>

The western United States has been experiencing severe drought since 2013. The solid earth response to the accompanying loss of surface and near-surface water mass should be a broad region of uplift. We use seasonally adjusted time series from continuously operating global positioning system stations to measure this uplift, which we invert to estimate mass loss. The median uplift is 5 millimeters (mm), with values up to 15 mm in California's mountains. The associated pattern of mass loss, ranging up to 50 centimeters (cm) of water equivalent, is consistent with observed decreases in precipitation and streamflow. We estimate the total deficit to be ~240 gigatons, equivalent to a 10-cm layer of water over the entire region, or the annual mass loss from the Greenland Ice Sheet.

Over the past few years, the western continuous United States (WUSA) has experienced large interannual variations in hydrological conditions and is currently undergoing a severe drought. Coincident observations of reduced precipitation and streamflow reflect the impact of the drought but do not directly measure the associated deficit in terrestrial water storage (TWS), which is a comprehensive metric that includes cumulative changes

in vegetation and soil moisture, perennial snow and ice, groundwater, and surface water. Satellite gravity measurements from NASA's Gravity Recovery and Climate Experiment (GRACE) have been widely used to observe TWS (1, 2), though these results indicate that for transient signals the intrinsic spatial resolution of these measurements is several hundred kilometers. Additional information about TWS at higher resolution is needed to understand the extent and impact of the current drought at basin to regional scales across the WUSA.

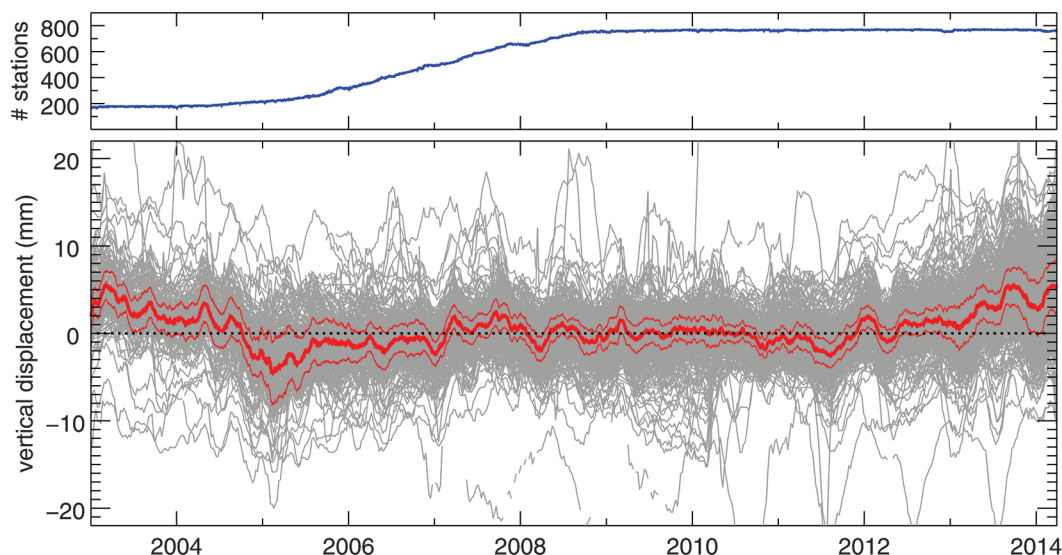
Like other varying loads on Earth's surface, the water mass loss associated with the drought will induce instantaneous vertical and horizontal dis-

placements from elastic deformation (3). These can be measured at the millimeter level using the Global Positioning System (GPS), which has been done for seasonal changes in snowpack (4) and in hydrologic systems such as lakes (5, 6) and river basins (7, 8). Except very close to the load, these displacements are largely independent of local structure (e.g., sedimentary basins behave the same as bedrock). Displacements from loading provide information about changes at intermediate spatial scales not otherwise observable, and they integrate the effects of all loads—an advantage because displacements provide data from areas otherwise not measured, and a challenge because inversion is required to find the actual spatial distribution.

To study the loading response corresponding to hydrological changes, we have analyzed the past 11 years (2003 to 2014) of daily vertical positions estimated for continuous GPS stations from the National Science Foundation's Plate Boundary Observatory (PBO) and several smaller networks. The stations we used were located on the U.S. mainland west of longitude 109°W and on Vancouver Island. We detrended each time series to remove secular tectonic motion and used the seasonal-trend-loess (STL) method (9) to remove seasonal signals due to water loading (10–12). The STL method is effective on time series like GPS that exhibit modulated behavior (13, 14) that is not well represented by annual and semiannual sinusoids (fig. S1).

GPS records transient displacements from phenomena other than surface loading, including volcanic or tectonic forcing (15) and the

**Fig. 1. Vertical GPS displacement time series.** Detrended and seasonally adjusted daily vertical displacements from 771 continuous GPS stations in the WUSA, decimated to weekly intervals for plotting (gray lines). The thick red line is the median value of all data for each day, and the light red lines indicate the SD computed from the interquartile range. The uplift that began in 2013 is notable for the period after 2006, when the number and distribution of GPS stations greatly expanded across the region with the building of the PBO (blue line shows the number of stations used in the analysis).



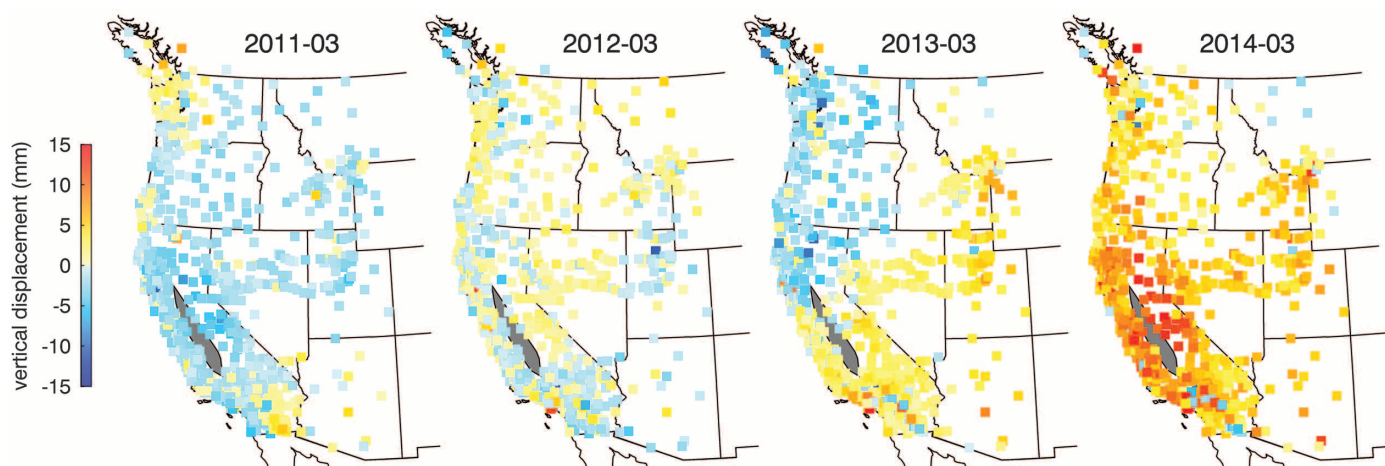


**Fig. 2. Maps of vertical GPS displacements.** Spatial distribution of displacements from the time series in Fig. 1, from 1 March 2011 through 2014. Uplift is indicated by yellow-red colors and subsidence by shades of blue. The gray region is where stations were excluded in the Central Valley of California.

poroelastic response of aquifers to groundwater extraction and recharge (16, 17). In addition, fictitious vertical displacements can be caused by variations in the signal-scattering environment close to each station (18), but these “multipath” effects contribute, on average, only a few millimeters of correlated noise to daily position estimates (19) and are not expected to substantially affect our results. We mitigated the impact of nonloading signals by excluding all stations within the actively deforming Long Valley caldera (20); all stations in California’s Central Valley, where agricultural pumping is widespread (21, 22); stations whose seasonal displacements suggest they are located above an actively pumped aquifer (17); and a few gross outliers (12).

After removing these stations, we were left with 771 GPS displacement time series (12) for our analysis. The median vertical displacement over time reveals a period of uplift beginning in 2013 and continuing through the present (Fig. 1). Before 2013, the median displacement did not deviate more than a few millimeters from zero, at least not since the mid-2005 inception of the PBO network. (We attribute the variability before 2006 to the much smaller number of stations and their concentration in southern California.) Vertical motion in the region is much more dynamic than this overall stability might suggest, as shown by the spatial pattern of displacements (Fig. 2). In March 2011, widespread but modest subsidence prevailed over most of the WUSA, but this had changed to spatially random uplift and subsidence by March 2012. By March 2013, moderate subsidence had returned to the Pacific Northwest and northern California, while moderate uplift had begun elsewhere. A year later, in March 2014, uplift had dramatically increased in California and was widespread across the entire WUSA.

These results demonstrate that interannual vertical displacements vary considerably from year to year, even when the WUSA as a whole is stable. Examining the data at weekly intervals reveals that the spatial displacement patterns

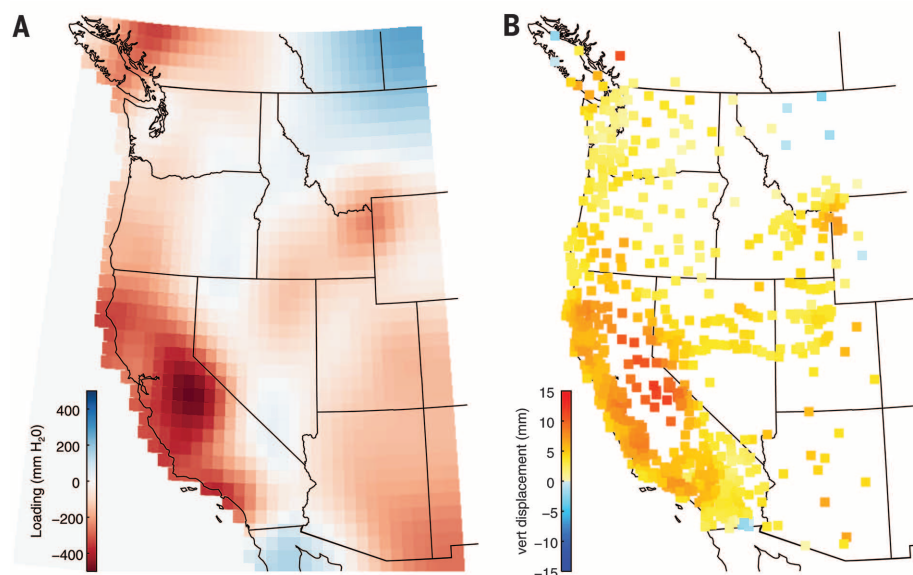


**Fig. 3. Maps of estimated loads and predicted displacements.** (A) Loading estimate for the WUSA in March 2014. Redder areas indicate negative loading (mass deficit), bluer areas indicate positive loading (mass surplus), and white areas are unchanged. (B) Vertical displacements, corresponding to the loading model in (A), at the locations of the GPS stations used in this analysis (compare to actual displacements in rightmost panel of Fig. 2).

shown in Fig. 2 evolve coherently over the entire period of analysis on scales of 100 to 1000 km. This behavior is inconsistent with GPS processing error, which would typically cause random noise or motion of the entire network, or with groundwater extraction, which primarily affects agricultural or urban areas (17). The GPS stations in our analysis are either attached to solid rock or anchored at several meters depth in soils, so poroelastic effects due to changes in surface soil water content should not affect our results. Finally, interannual horizontal GPS displacements in the region are typically much smaller than their vertical counterparts (Fig. 2 and figs. S2 and S3), which is inconsistent with both volcanic and tectonic processes (6, 23). The only process that can reasonably account for the observed broad-

scale deformation is spatiotemporal variation in loading.

We used the observed GPS displacements in March 2014 to estimate the distribution of loads on a  $0.5^\circ$  grid spanning the WUSA. We calculated the vertical displacement at each station for surface loads on an elastic Earth (3, 24, 25) and used these to invert for loads on the grid (12), applying a regularization constraint to balance model misfit and smoothness. Predicted displacements from our preferred load model (Fig. 3) reduce the root mean square of the observed displacements by 53% (fig. S7) and yield spatially random residuals. A checkerboard test (fig. S8) suggests that the spatial resolution of the model is 200 to 300 km, except at the northern and eastern edges of the GPS network, where station spacing is larger.



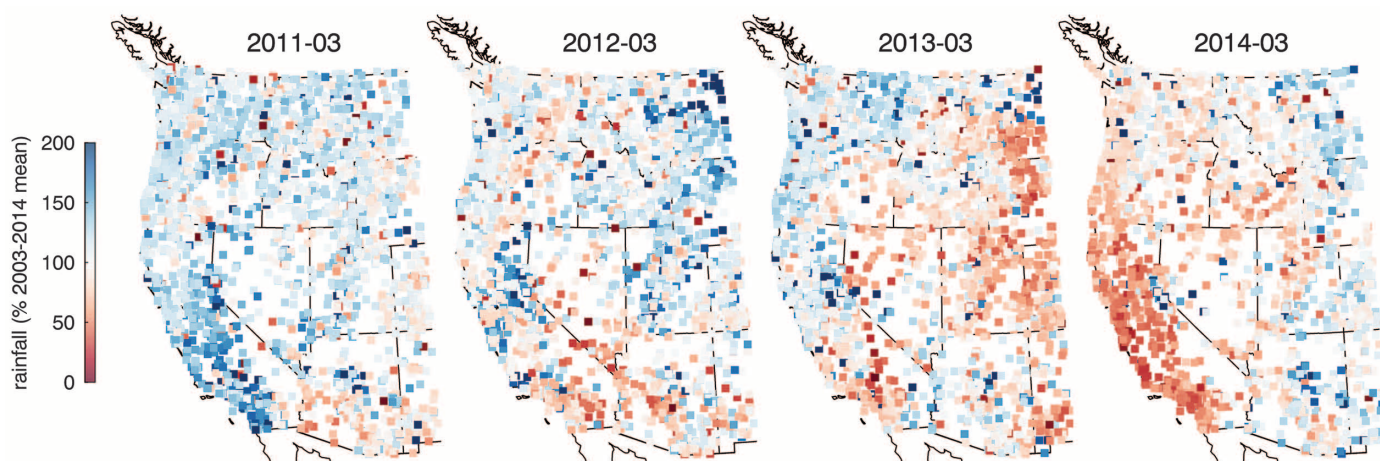


**Fig. 4. Maps of annual precipitation anomalies.** Deviation of annual precipitation from the 2003-to-2013 mean at meteorological stations in the National Oceanic and Atmospheric Administration's Global Historical Climatology Network, for 2011 to 2014. The pattern of precipitation—in particular, the surplus in California in 2011 and the deficit in 2014—mirrors the pattern of uplift seen in the GPS data.

The inversion produces an estimate of the load that resembles the uplift pattern but is smoother because of the constraints imposed. In March 2014, when most vertical displacements are farthest from their long-term averages, our results show crustal unloading over the entire WUSA, with a maximum in the central Sierra Nevada equivalent to 50 cm of water (Fig. 3). There appears to be a small amount of real non-tectonic loading in Montana, whereas the apparent loading just south of the U.S.-Mexico border is probably caused by postseismic effects from the moment magnitude 7.2 El Mayor-Cucapah earthquake in 2010 (26). The arid regions of eastern California, Oregon, Washington, and western Nevada show little loading. Estimated loads near the northern and southern boundaries of the grid, as well as in Arizona, Utah, and Montana, are poorly constrained by the GPS data.

We interpret the widespread negative loading, with its central California maximum, to represent changes in terrestrial water storage due to the current WUSA drought. The implied drying relative to the long-term mean appears to be most acute in coastal and mountainous areas and subdued in highly arid regions. This is expected, because the change in precipitation in a drought is proportional to the climatological mean value, so that arid regions lose less water than do wet regions. The area-integrated water deficit over the WUSA in March 2014 is 240 gigatons, a value that is insensitive to the degree of smoothing used in the inversion (fig. S6). For perspective, this deficit is equivalent to a uniform 10-cm layer of water over the entire WUSA and is the magnitude of the current annual mass loss from the Greenland Ice Sheet.

The temporal and spatial water storage variations implied by the observed displacements are consistent with contemporaneous observations of precipitation and streamflow, all of which underscore the extent and severity of the current drought in the WUSA. The departure of annual precipitation from the long-term average (Fig. 4)

highlights the changes over the past few years: a wet 2011; a variable 2012; a dry 2013 for the western Rockies, the Great Basin, and parts of California; and severe drought in 2014 along the Pacific coast, with dry conditions extending inland to the Rocky Mountains. Precipitation patterns in 2011 and 2014, in particular, match the pattern of vertical displacements for, respectively, excess (wet) and deficit (dry) loading conditions. Streamflow data from the U.S. Geological Survey (USGS) stream gauge network (fig. S9) exhibit wet/dry patterns similar to the precipitation data, although it is the years 2013 and 2014 that most closely match the vertical displacements. These data sets are consistent with each other and also complementary, each highlighting a different component of the hydrological system.

It has been suggested that long-term and seasonal variations in mass loading due to the hydrological cycle may affect seismicity rates along the San Andreas fault (27). We computed the Coulomb stress change on the San Andreas fault from the load shown in Fig. 3 (22, 28) and found that the past 2 years of unloading have increased Coulomb stresses by 100 to 200 Pa, approximately the same amount as a week of tectonic strain accumulation (29). Therefore, stress changes from the drought unloading seem unlikely to affect seismicity.

Other methods that can directly monitor changes in total water mass change are sensitive to different spatial scales. Gravimeters allow very sensitive detection of mass changes, but because their sensitivity falls off as  $r^{-2}$  (where  $r$  is the distance to the mass), they are best at measuring very local changes (30). Conversely, perturbations to satellite orbits can be used to detect changing mass distributions over the whole Earth but are insensitive to load variations with wavelengths much less than the orbital height. The nominal resolution for the GRACE satellite is 400 to 500 km (31), which is consistent with results from GRACE studies of drought-induced mass changes (1, 2). For vertical displacements from GPS, the loading Green function varies as  $r^{-1}$ : Load-induced sig-

nals reflect both local and regional changes. Combining these different measurement types offers the greatest promise for monitoring terrestrial water storage.

In the WUSA, interannual changes in crustal loading are driven by changes in cool-season precipitation, which cause variations in surface water, snowpack, soil moisture, and groundwater. We have demonstrated that GPS can be used to recover loading changes due to both wet (e.g., 2011) and dry (e.g., post-2013) climate patterns, which suggests a new role for GPS networks such as that of the PBO. Although precipitation and surface water levels are currently well sampled, other components of terrestrial water storage are monitored only at a limited number of locations, including a growing number of GPS stations for which GPS reflectometry measurements of snow depth and soil moisture are available (32–34). Our analysis shows that the existing network of continuous GPS stations in the WUSA measures vertical crustal motion at sufficient precision and sampling density to allow the estimation of interannual changes in water loads, providing a new view of the ongoing drought in much of the WUSA. Furthermore, the exceptional stability of the GPS monumentation (35) means that this network is also capable of monitoring the long-term effects of regional climate change. Surface displacement observations from GPS, in the WUSA and globally, have the potential to dramatically expand the capabilities of the current hydrological observing network, and continued operation of these instruments will provide considerable value in understanding current and future hydrological changes, with obvious social and economic benefits.

#### REFERENCES AND NOTES

1. F. Frappart et al., *Environ. Res. Lett.* **7**, 044010 (2012).
2. A. C. Thomas, J. T. Reager, J. S. Famiglietti, M. Rodell, *Geophys. Res. Lett.* **41**, 1537–1545 (2014).
3. W. E. Farrell, *Rev. Geophys.* **10**, 761–797 (1972).
4. K. J. Ouellette, C. de Linage, J. S. Famiglietti, *Water Resour. Res.* **49**, 2508–2518 (2013).
5. P. Elósegui, J. L. Davis, J. X. Mitrovica, R. A. Bennett, B. P. Wernicke, *Geophys. Res. Lett.* **30**, 1111 (2003).

6. J. Wahr *et al.*, *J. Geophys. Res.* **117**, 1795–1806 (2013).
7. M. Bevis *et al.*, *Geophys. Res. Lett.* **32**, L16308 (2005).
8. P. Bettinelli *et al.*, *Earth Planet. Sci. Lett.* **266**, 332–344 (2008).
9. R. B. Cleveland, W. S. Cleveland, J. E. McRae, I. Terpenning, *J. Off. Stat.* **6**, 3–73 (1990).
10. M. S. Steckler *et al.*, *J. Geophys. Res.* **115**, B08407 (2010).
11. D. Argus, Y. Fu, F. Landerer, *Geophys. Res. Lett.* **41**, 1971–1980 (2014).
12. Materials and methods are available as supplementary materials on Science Online.
13. R. A. Bennett, *Geophys. J. Int.* **174**, 1052–1064 (2008).
14. J. L. Davis, B. P. Wernicke, M. E. Tamisiea, *J. Geophys. Res.* **117**, B01403 (2012).
15. D. Dzurlin, *Volcano Deformation: Geodetic Monitoring Techniques* (Springer, New York, 2007).
16. N. E. King *et al.*, *J. Geophys. Res.* **112**, B03409 (2007).
17. D. L. Galloway, T. J. Burbey, *Hydrogeol. J.* **19**, 1459–1486 (2011).
18. P. Elósegui *et al.*, *J. Geophys. Res.* **100**, 9921–9934 (1995).
19. M. A. King *et al.*, *Surv. Geophys.* **31**, 465–507 (2010).
20. K.-H. Ji, T. A. Herring, A. L. Llenos, *Geophys. Res. Lett.* **40**, 1054–1058 (2013).
21. M. E. Ikehara, *Hydrol. Sci. J.* **39**, 417–429 (1994).
22. R. T. Hanson *et al.*, in *Land Subsidence, Associated Hazards, and the Role of Natural Resources Development* (International Association of Hydrological Sciences Press, Wallingford, UK, 2010), vol. 339, pp. 467–471.
23. R. Grapenthin, B. G. Ofeigsson, F. Sigmundsson, E. Sturkell, A. Hooper, *Geophys. Res. Lett.* **37**, L20310 (2010).
24. D. C. Agnew, in *Treatise on Geophysics: Geodesy*, T. A. Herring, Ed. (Elsevier, New York, 2007), pp. 163–195.
25. D. C. Agnew, “SPOTL: Some Programs for Ocean-Tide Loading” (SIO Technical Report, Scripps Institution of Oceanography, La Jolla, CA, 2012); <http://escholarship.org/uc/item/954322pg>.
26. F. Pollitz, R. Bürgmann, W. Thatcher, *Geochem. Geophys. Geosyst.* **13**, Q06002 (2012).
27. C. B. Amos *et al.*, *Nature* **509**, 483–486 (2014).
28. L. Astiz, P. M. Shearer, D. C. Agnew, *J. Geophys. Res.* **105**, 2937–2953 (2000).
29. B. Smith-Konter, D. Sandwell, P. M. Shearer, *J. Geophys. Res.* **116**, B06401 (2011).
30. M. Van Camp, O. de Viron, L. Métivier, B. Meurers, O. Francis, *Geophys. J. Int.* **197**, 192–201 (2014).
31. G. Ramillien, J. S. Famiglietti, J. Wahr, *Surv. Geophys.* **29**, 361–374 (2008).
32. K. M. Larson *et al.*, *IEEE J. Select. Top. Appl. Earth Obs. Remote Sens.* **3**, 91–99 (2010).
33. E. D. Gutmann, K. M. Larson, M. W. Williams, F. G. Nievenski, V. Zavorotny, *Hydrol. Processes* **26**, 2951–2961 (2012).
34. W. Wan, K. M. Larson, E. E. Small, C. C. Chew, J. J. Braun, *GPS Solut.* **10.1007/s10291-014-0383-7** (2014).
35. J. O. Langbein, F. Wyatt, H. Johnson, D. Hamann, P. Zimmer, *Geophys. Res. Lett.* **22**, 3533–3536 (1995).

## ACKNOWLEDGMENTS

The GPS data we use come primarily from the PBO and are publicly available from UNAVCO through the Geodesy Advancing Geosciences and EarthScope Facility, which is supported by the NSF and NASA under NSF cooperative agreement no. EAR-1261833. Meteorological data are publicly available from the National Climatic Data Center's Global Historical Climatology Network. The software used for load computation (SPOTL) is publicly available, and the processing software may be obtained from us. We acknowledge the efforts of many at UNAVCO to produce the exceptional PBO GPS data set, especially the station installation efforts of C. Walls, K. Austin, and K. Feaux. We thank M. Dettinger for comments. This work was supported by USGS grant no. G13AP00059.

## SUPPLEMENTARY MATERIALS

[www.sciencemag.org/content/345/6204/1587/suppl/DC1](http://www.sciencemag.org/content/345/6204/1587/suppl/DC1)

Materials and Methods

Figs. S1 to S9

References

20 June 2014; accepted 8 August 2014

Published online 21 August 2014;

10.1126/science.1260279

## EARLY SOLAR SYSTEM

# The ancient heritage of water ice in the solar system

L. Ilseore Cleeves,<sup>1\*</sup> Edwin A. Bergin,<sup>1</sup> Conel M. O'D. Alexander,<sup>2</sup> Fujun Du,<sup>1</sup> Dawn Graninger,<sup>3</sup> Karin I. Öberg,<sup>3</sup> Tim J. Harries<sup>4</sup>

Identifying the source of Earth's water is central to understanding the origins of life-fostering environments and to assessing the prevalence of such environments in space. Water throughout the solar system exhibits deuterium-to-hydrogen enrichments, a fossil relic of low-temperature, ion-derived chemistry within either (i) the parent molecular cloud or (ii) the solar nebula protoplanetary disk. Using a comprehensive treatment of disk ionization, we find that ion-driven deuterium pathways are inefficient, which curtails the disk's deuterated water formation and its viability as the sole source for the solar system's water. This finding implies that, if the solar system's formation was typical, abundant interstellar ices are available to all nascent planetary systems.

Water is ubiquitous across the solar system, in cometary ices, terrestrial oceans, the icy moons of the giant planets, and the shadowed basins of Mercury (1, 2). Water has left its mark in hydrated minerals in meteorites, in lunar basalts (3), and in martian melt inclusions (4). The presence of liquid water facilitated the emergence of life on Earth; thus, understanding the origin(s) of water throughout the solar system is a key goal of astrobiology. Comets and asteroids (traced by meteorites) remain the most primitive objects, providing a natural “time capsule” of the conditions present during the epoch of planet formation. Their compositions reflect those of the gas,

dust, and—most important—ices encircling the Sun at its birth, i.e., the solar nebula protoplanetary disk. There remain open questions, however, as to when and where these ices formed, whether they (i) originated in the dense interstellar medium (ISM) in the cold molecular cloud core before the Sun's formation or (ii) are products of reprocessing within the solar nebula (5–7). Scenario (i) would imply that abundant interstellar ices, including water and presolar organic material, are incorporated into all planet-forming disks. By contrast, local formation within the solar nebula in scenario (ii) would potentially result in large water abundance variations from stellar system to system, dependent on the properties of the star and disk.

In this work, we aim to constrain the formation environment of the solar system's water, using deuterium fractionation as our chemical tracer. Water is enriched in deuterium relative to hydrogen (D/H) compared with the initial bulk solar composition across a wide range of solar system bodies, including comets, (8, 9), terrestrial and ancient martian water (4), and hydrated minerals in meteorites (10). The amount of deu-

terium relative to hydrogen of a molecule depends on its formation environment; thus, the D/H fraction in water,  $[D/H]_{H_2O}$ , can be used to differentiate between the proposed source environments. Interstellar ices, as revealed by sublimation in close proximity to forming young stars, also exhibit high degrees of deuterium enrichment, ~2 to 30 times that of terrestrial water (11–14). It is not known to what extent these extremely deuterated interstellar ices are incorporated into planetesimals or if, instead, the interstellar chemical record is erased by reprocessing during the formation of the disk (15, 16). Owing to water's high binding energy to grain surfaces, theoretical models predict that water is delivered from the dense molecular cloud to the disk primarily as ice, with some fraction sublimated at the accretion shock in the inner tens of astronomical units (AU) (15). If a substantial fraction of the interstellar water is thermally reprocessed, the interstellar deuterated record could then be erased. In this instance, the disk is left as primary source for (re-)creating the deuterium-enriched water present throughout our solar system.

The key ingredients necessary to form water with high D/H are cold temperatures, oxygen, and a molecular hydrogen ( $H_2$ ) ionization source. The two primary chemical pathways for making deuterated water are (i) gas-phase ion-neutral reactions, primarily through  $H_2D^+$  and (ii) grain-surface formation (ices) from ionization-generated hydrogen and deuterium atoms from  $H_2$ . Both reaction pathways depend critically on the formation of  $H_2D^+$ . In particular, the gas-phase channel (i) involves the reaction of  $H_2D^+$  ions with atomic oxygen or OH through a sequence of steps to form  $H_2DO^+$ , which recombines to form a water molecule. The grain-surface channel (ii) is powered by  $H_2D^+$  recombination with electrons or grains, which liberates hydrogen and deuterium atoms that react with oxygen atoms on cold dust grains.  $H_2D^+$  becomes enriched relative to  $H_3^+$  because the deuterated isotopologue is energetically favored at low temperatures. There is

<sup>1</sup>Department of Astronomy, University of Michigan, 311 West Hall, 1085 South University Avenue, Ann Arbor, MI 48109, USA. <sup>2</sup>Department of Terrestrial Magnetism, Carnegie Institution of Washington, Washington, DC 20015, USA.

<sup>3</sup>Harvard-Smithsonian Center for Astrophysics, Harvard University, Cambridge, MA 02138, USA. <sup>4</sup>Department of Physics and Astronomy, University of Exeter, Stocker Road, Exeter EX4 4QL, UK.

\*Corresponding author. E-mail: cleeves@umich.edu.